SACLANTCEN REPORT
serial no: SR- 333

SACLANT UNDERSEA RESEARCH CENTRE REPORT

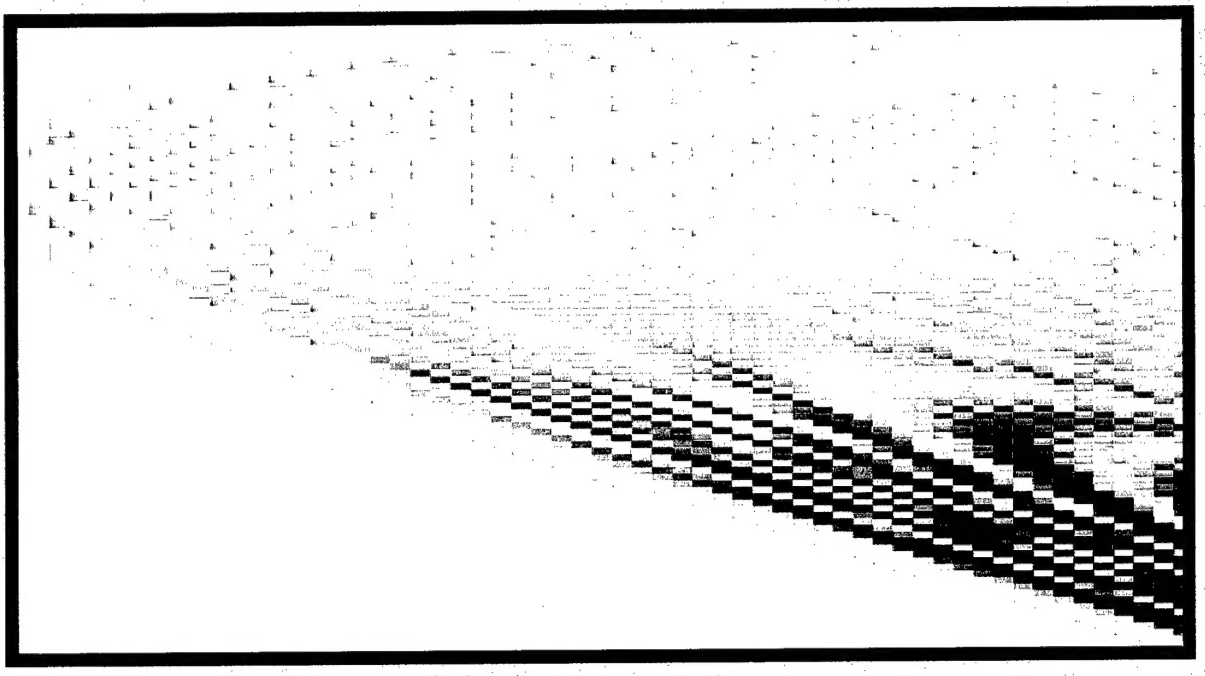

NORTH ATLANTIC TREATY ORGANIZATION ORGANISATION DU TRAITE DE L'ATLANTIQUE NORD

SACLANTCEN SR-333

Theoretical and Numerical Issues in Travel Time Tomography

B. Edward McDonald,

Brian Sperry* and Arthur B. Baggeroer*

*MIT, Cambridge MA

The content of this document pertains to work performed under Project 01-A of the SACLANTCEN Programme of Work. The document has been approved for release by The Director, SACLANTCEN.

Jan L. Spoelstra
Director

intentionally blank page

Theoretical and Numerical Issues in Travel Time Tomography

B. Edward McDonald,

Brian Sperry* and Arthur B. Baggeroer*

Executive Summary: Ocean tomography involves use of long range sound transmission to probe a region of interest. The resulting receptions on a vertical array are processed with appropriate inversion methods to reveal properties of the ocean's sound speed and thermal structure. The theoretical framework for such inversion methods have produced some mathematical questions concerning the methods' consistency and range of accuracy. This report documents progress in quantifying the consistency and accuracy of some of the methods. The work presented here may also be extended to more recent problems involving shallow water and geoacoustic inversion.

*MIT, Cambridge MA

intentionally blank page

Theoretical and Numerical Issues in Travel Time Tomography

B. Edward McDonald,

Brian Sperry* and Arthur B. Baggeroer*

Abstract: Results from perturbation theory for changes in ocean acoustic modal group speeds due to small environmental changes are investigated with regard to their applicability to inversion schemes for large scale trends in the ocean's thermal structure. In regions where adiabatic mode theory is applicable, the inverse problem for each vertical eigenmode consists of an integral equation whose kernel involves the eigenfunction and its frequency derivative. We give a proof for the so called 'third term problem' which requires equivalence between two dissimilar integrals relating the perturbations in the water column, the resulting perturbations in the acoustic eigenmode under consideration, and the frequency derivative of the eigenmode. We give numerical examples for the inversion kernel for four types of sound speed profiles, and then explore numerically the parameter range (amplitude and scale size) in which perturbation theory is accurate.

Keywords: perturbation theory ∘ acoustic inversion ∘ ocean tomography

*MIT, Cambridge MA

Contents

1

Introduction

Perturbative approaches to ocean acoustic tomography [1, 2, 3] seek to estimate changes in an assumed basic ocean state by measuring perturbations in acoustic transmission properties. Large scale ocean experiments (*e.g.*, HIFT[4], ATOC[5] and SLICE89[6]) have recorded pulse arrivals on vertical hydrophone arrays, yielding large amounts of path- integrated acoustic information concerning the state of the ocean. A physically revealing way to display and/or process this information is to employ modal filters[7, 8] and modal group travel time tomography.

Modal group travel time tomography relates arrival time information for individual acoustic eigenmodes to details of sound speed structure in the water column[2] or ocean bottom[9] within a vertical slice taken along a presumed horizontal path. In the current work we investigate theoretical and numerical issues involving the adequacy of perturbative methods to calculate modal group slowness changes resulting from imposed perturbations in the water column. We assume sufficiently weak range dependence so as to allow the use of adiabatic normal mode theory.

We will show that two independent derivations of perturbed modal group slowness which appear to give different results[10] are actually consistent, as a result of a reciprocity principle in Sturm- Liouville systems. The search for an adequate proof of this consistency has been referred to as the 'third term problem'.

We then investigate issues involved in the evaluation of the frequency derivative of the acoustic eigenmode $\partial\psi_n(z,\omega)/\partial\omega$. This quantity plays a central role in perturbative inversion. In previous approaches [2, 3, 9, 11] one solves the appropriate eigenvalue problem at two neighboring frequencies and evaluates the frequency derivative by finite differences[12]. Finite differences may be sensitive to iteration errors at high mode numbers or in situations where the two eigenvalue solutions converge slowly. We offer an independent method in which an equation for $\partial\psi_n/\partial\omega$ is solved directly.

We cast the perturbative inverse as a least squares problem, and derive numerical estimates for the appropriate inversion kernel[13]. Our approach is consistent with the range integrated formulation of Shang[3], allowing for different methods of evaluating $\partial\psi_n/\partial\omega$. Rather than give sample inversions of synthetic data for a single "canonical" sound speed profile as did Shang[3], we give numerical examples of the

perturbative inversion kernel for the canonical profile and three other types of sound speed profiles (SSP): a smooth mid- latitude SSP, a mostly upward refracting high latitude SSP with strong surface interaction, and a double- ducted high latitude SSP.

Next we investigate numerically the parameter range in which linear perturbation theory yields accurate results for modal group slowness. In particular, we give numerical examples for the canonical profile in which the error in the perturbation method is calculated as a function of the amplitude and vertical extent of assumed perturbations in the water column.

2
Theory

In a weakly range dependent ocean environment, the acoustic field is described by adiabatic mode theory with vertical eigenmodes $\psi_n(z;x,y)$ where the vertical coordinate is z, and the dependence of the environment on (x,y) is weak. The eigenmodes ψ_n satisfy

$$\rho\frac{\partial}{\partial z}\left(\rho^{-1}\frac{\partial\psi_n}{\partial z}\right)+\frac{\omega^2}{c^2(z;x,y)}\,\psi_n=\kappa_n^2(x,y)\,\psi_n, \tag{1}$$

with orthonormality

$$\left(\psi_n,\ \ \psi_m\right)=\delta_{n,m} \tag{2}$$

where $\delta_{n,m}$ is the Kronecker delta symbol

$$\delta_{n,m}=\begin{cases}1 & m=l\\ 0 & m\neq l.\end{cases}$$

Boundary conditions are $\psi_n=0$ at the pressure release surface $z=0$, and $\psi_n\to 0$ for $z\to-\infty$, corresponding to mode trapping. In equation (1) ρ is density (allowing for stratification in the ocean bottom), and the inner product $(*\ ,\ *)$ in (2) is

$$\left(A,\ \ B\right)\equiv\int\rho^{-1}A\,B\,dz. \tag{3}$$

For notational convenience we define slowness as the reciprocal of sound speed:

$$s(z;x,y)\equiv c(z;x,y)^{-1}, \tag{4}$$

so that for a time harmonic signal of radian frequency ω the wavenumber field is

$$k(z;x,y)=\omega s(z;x,y). \tag{5}$$

We represent (1) symbolically as

$$L\,\psi_n=\kappa_n^2(x,y)\,\psi_n, \tag{6}$$

where the linear operator L is

$$L=\rho\partial_z\rho^{-1}\partial_z+\omega^2 s^2(z;x,y). \tag{7}$$

With the stated boundary conditions and real sound speed (no attenuation in the basic state) the operator L is self adjoint.

We will supress the weak (x, y) dependence in what follows, so that functions $f(z)$ really represent $f(z; x, y)$.

From (1) one has for the square of the modal horizontal wavenumber,

$$\kappa_n^2(x, y) = (\psi_n, L\psi_n) \tag{8}.$$

2.1 Acoustic Inversion and the Curious 'Third Term Problem'

From equation (8) we may derive expressions relating assumed perturbations $\delta s(z)$ in the water column sound slowness to the resulting changes in modal group slowness. Inversion schemes then attempt to relate variations in modal travel times (and thus modal group slowness) to the water column variations $\delta s(z; x, y)$. One can either perturb (8) with respect to δs and then take a frequency derivative, or take the frequency derivative of (8) and then perturb with respect to δs. Following these different paths leads to very different looking results [10]; part of the goal of the present paper is to show that they are indeed the same.

2.1.1 Frequency Derivative of the Perturbed System

Upon perturbing the sound slowness profile while keeping the ocean depth constant, $s \to s + \delta s$ one has from (8)

$$\begin{aligned} 2\kappa_n \delta\kappa_n &= \Big(\psi_n, L\delta\psi_n\Big) + \Big(\delta\psi_n, L\psi_n\Big) + 2\omega^2\Big(\psi_n, s\delta s\psi_n\Big) \\ &= 2\kappa_n^2\Big(\psi_n, \delta\psi_n\Big) + 2\omega^2\Big(\psi_n, s\delta s\psi_n\Big) \end{aligned} \tag{9}$$

where we have invoked (6) in the second expression. Orthonormality (2) requires that the first term on the right hand side of the second expression be zero, so that the perturbation in the horizontal wavenumber is

$$\delta\kappa_n = \frac{\omega^2}{\kappa_n}\Big(\psi_n, s\delta s\psi_n\Big). \tag{10}$$

The frequency derivative of (10) gives

$$\begin{aligned}\frac{\partial}{\partial\omega}\delta\kappa_n &\equiv \delta s_n^g \\ &= \Big(2\frac{\omega}{\kappa_n} - \frac{\omega^2}{\kappa_n^2}\frac{\partial\kappa_n}{\partial\omega}\Big)\Big(\psi_n, s\delta s\psi_n\Big) + 2\frac{\omega^2}{\kappa_n}\Big(\psi_n, s\delta s\frac{\partial\psi_n}{\partial\omega}\Big),\end{aligned} \tag{11}$$

where δs_n^g refers to the perturbation in the modal group slowness of mode n. Equation (11) gives the following integral for the perturbed group slowness:

$$\delta s_n^g = \frac{\omega}{\kappa_n}\int \rho^{-1}\Big((2 - \frac{\omega}{\kappa_n}s_n^g)\psi_n^2 + 2\omega\psi_n\frac{\partial\psi_n}{\partial\omega}\Big)s\delta s dz. \tag{12}$$

Equation (12) relates the perturbation in modal group slowness to the change δs in the slowness distribution in an expression which requires knowledge of the eigenfunction, its frequency derivative, and unperturbed modal parameters κ_n and $s_n^g \equiv \partial\kappa_n/\partial\omega$. The perturbation $\delta\psi_n$ in the eigenfunction does not appear in (12), having been eliminated by orthonormality.

2.1.2 *Perturbation of the Frequency Derivative*

Returning to (8), a frequency derivative gives

$$2\kappa_n s_n^g = 2\Big(\frac{\partial\psi_n}{\partial\omega}, L\psi_n\Big) + 2\omega\Big(\psi_n^2, s^2\Big) \tag{13}$$

The first term on the right is again zero due to (1) and orthonormality. The modal group slowness is thus

$$s_n^g = \frac{\omega}{\kappa_n}\Big(\psi_n^2, s^2\Big) \tag{14}$$

Perturbing (14) with respect to δs now gives

$$\begin{aligned}\delta s_n^g &= 2\frac{\omega}{\kappa_n}\Big[\Big(\psi_n, s^2\delta\psi_n\Big) + \Big(\psi_n, s\delta s\psi_n\Big)\Big] - \delta\kappa_n\frac{\omega}{\kappa_n^2}\Big(\psi_n^2, s^2\Big) \\ &= \frac{\omega}{\kappa_n}\int \rho^{-1}dz\Big((2 - s_n^g\frac{\omega}{\kappa_n})\psi_n^2 s\delta s + 2s^2\psi_n\delta\psi_n\Big).\end{aligned} \tag{15}$$

The second expression here results from (10) and (14). Equation (15) gives the change in the modal group slowness due to δs in an expression requiring knowlege of eigenfunction, its response $\delta\psi_n$, and and unperturbed modal parameters κ_n and s_n^g. The frequency derivative term in (13) is eliminated by orthonormality.

Equations (12) and (15) must give identical results for physical consistency, but they differ in each of their third terms. Consistency of the third terms of (12) and (15)

requires that the following general relation hold among the eigenfunction, its frequency derivative, the imposed sound slowness perturbation, and the eigenfunction's response to the perturbation:

$$\int \rho^{-1} s(z)^2 \psi_n \delta\psi_n dz \stackrel{?}{=} \omega \int \rho^{-1} s(z) \psi_n \frac{\partial \psi_n}{\partial \omega} \delta s(z) dz \tag{16}$$

Equation (16) is a curious and unexpected relation that has been called the 'third term problem.' It points to a fundamental but not obvious role played by the eigenmode's frequency derivative in relating the water column perturbation δs to the eigenmode's response $\delta\psi_n$. The importance of this frequency derivative term in synthesizing time domain pulses using a narrow band approximation has been established recently in numerical studies by LePage[14].

2.2 *Reciprocity in Perturbed Sturm- Liouville Systems*

We will show that equation (16) is *not* a constraint on the perturbations, but an example of a general property of Sturm- Liouville eigenvalue problems of the form $L\psi_n = \lambda_n \psi_n$ with orthonormality $(\psi_n, \psi_m) = \delta_{n,m}$. Let us represent the system and its linear perturbation as

$$L\psi_n = \lambda_n \psi_n \tag{17a}$$

$$L\ \delta\psi_n + \delta L\ \psi_n = \lambda_n\ \delta\psi_n + \delta\lambda_n\ \psi_n, \tag{17b}$$

and thus

$$(L - \lambda_n)\, \delta\psi_n = (\delta\lambda_n - \delta L)\, \psi_n. \tag{18}$$

The left hand side of this equation is orthogonal to ψ_n, so that the right hand side must be also. As a result,

$$\delta\lambda_n = (\psi_n, \delta L\ \psi_n). \tag{19}$$

Since the Sturm- Liouville eigenvalues λ_n are distinct, the operator $(L - \lambda_n)$ has no zeros on the vector space $\mathbf{R}_{\perp n} \equiv \{\psi_j, j \neq n\}$ orthogonal to ψ_n. Thus from (18)

$$\begin{aligned} \delta\psi_n &= (L - \lambda_n)^{-1} (\delta\lambda_n - \delta L)\, \psi_n \\ &= -(L - \lambda_n)^{-1} (\delta L \psi_n)_{\perp n}, \end{aligned} \tag{20}$$

where the subscript $\perp_n$ refers to projection onto $\mathbf{R}_{\perp n}$ (or equivalently orthogonalization to ψ_n).

Now consider two linearly independent perturbations of the system $\delta L^{(j)}, j = 1, 2$ with responses $\delta\psi_n^{(j)}, j = 1, 2$ in the eigenfunctions. Consider the following cross

term between perturbations and responses resulting from (20):

$$\begin{aligned}\left(\delta\psi_n^{(1)}, \delta L^{(2)}\psi_n\right) &= -\left((L-\lambda_n)^{-1}\left(\delta L^{(1)}\psi_n\right)_{\perp n}, \delta L^{(2)}\psi_n\right) \\ &= -\left(\delta L^{(1)}\psi_n, (L-\lambda_n)^{-1}\left(\delta L^{(2)}\psi_n\right)_{\perp n}\right) \\ &= \left(\delta\psi_n^{(2)}, \delta L^{(1)}\psi_n\right).\end{aligned} \tag{21}$$

In going from the first to second line of equation (21) we have invoked the self adjointness of the operator L and therefore of $(L-\lambda_n)^{-1}$. The latter expression on the right side of (21) differs from the first by only the interchange of indices. Thus

$$\left(\delta\psi_n^{(1)}, \delta L^{(2)}\psi_n\right) = \left(\delta\psi_n^{(2)}, \delta L^{(1)}\psi_n\right). \tag{22}$$

This statement of index interchangability between independent perturbations δL and $\delta\psi_n$ in the inner product (22) brings to mind the forcing - response reciprocity in many reversible physical systems.

2.3 Application to Tomographic Inversion

If we let $\delta L^{(1)}$ refer to a frequency perturbation $\delta\omega$ and $\delta L^{(2)}$ refer to a perturbation $\delta s(z)$ in the sound slowness profile, we have from (22) and (7)

$$\left(\delta\psi_n^{(1)}, 2\omega^2 s(z)\delta s(z)\psi_n\right) = \left(\delta\psi_n^{(2)}, 2\omega\ \delta\omega\ s^2(z)\psi_n\right). \tag{23}$$

Dividing both sides by $\delta\omega$, taking its limit to zero, and supressing superscript (2) for the eigenfunctions' response to the sound slowness perturbation we have

$$\left(\omega\frac{\partial\psi_n}{\partial\omega}, s(z)\delta s(z)\psi_n\right) = \left(\delta\psi_n, s(z)^2\psi_n\right), \tag{24}$$

which proves equation (16). We have thus established the equivalence of (12) and (15). To summarize, we have established that the perturbed group slowness may be calculated from either of the following equivalent expressions:

$$\begin{aligned}\delta s_n^g &= \frac{\omega}{\kappa_n}\int \rho^{-1}\Big((2-\frac{\omega}{\kappa_n}s_n^g)\psi_n^2 + 2\omega\psi_n\frac{\partial\psi_n}{\partial\omega}\Big)s\delta s dz \\ &= \frac{\omega}{\kappa_n}\int \rho^{-1}\Big((2-\frac{\omega}{\kappa_n}s_n^g)\psi_n^2\delta s + 2s\psi_n\delta\psi_n\Big)s\ dz.\end{aligned} \tag{25}$$

3

The Group Slowness Kernel $K_n(z)$

Returning to the issue of relating changes in group travel time to the sound slowness changes, one can derive from (20) an equation for the eigenfunction's frequency derivative. Let the perturbation be a change in frequency so that $\delta L = 2\omega\delta\omega s^2(z)$. Dividing by $\delta\omega$ and taking its limit to zero one has

$$\frac{\partial\psi_n}{\partial\omega} = -2\omega(L-\kappa_n^2)^{-1}\Big(s^2\psi_n\Big)_{\perp n} \tag{26}$$

so that from (12),

$$\delta s_n^g = \frac{\omega}{\kappa_n}\Big(2-\frac{s_n^g}{s_n^p}\Big)(\psi_n,\ s(z)\delta s(z)\psi_n) - 4\frac{\omega^3}{\kappa_n}\Big(\Big(L-\kappa_n^2\Big)^{-1}(s^2(z)\psi_n)_{\perp n},\ s(z)\delta s(z)\psi_n\Big) \tag{27}$$

where $s_n^p = \kappa_n/\omega$ is the modal phase slowness. One can rewrite (27) as in integral equation

$$\delta s_n^g = \int dz\ \delta s(z) K_n(z), \tag{28}$$

where

$$K_n(z) = \rho^{-1}\frac{\omega}{\kappa_n}\psi_n s(z)\Big\{\Big(2-\frac{s_n^g}{s_n^p}\Big)\psi_n - 4\omega^2(L-\kappa_n^2)^{-1}(s^2(z)\psi_n)_{\perp n}\Big\} \tag{29}$$

The shape of the kernel $K_n(z)$ determines the sensitivity of the modal group slowness to perturbations in slowness profile $\delta s(z)$.

Equation (28) gives the inverse problem for changes in the ocean sound slowness structure $\delta s(z)$. Arrival time data from a vertical array of sufficient resolution can be processed to yield changes δs_n^g in modal group speeds. Knowlege of the functions $K_n(z)$ determined from the unperturbed environment may be used in a least squares inversion of (28) to be given below.

Normalization of $K_n(z)$ is obtained by multiplying (29) by $c(z)$ and integrating. The second term in the curly brackets of (29) makes no contribution to the normalization, since it resides on $\mathbf{R}_{\perp n}$. The result is

$$s_n^p \int K_n(z)c(z)dz = \Big(2-\frac{s_n^g}{s_n^p}\Big). \tag{30}$$

For well- trapped modes group and phase speeds are very nearly equal, so that the right hand side of (30) is nearly unity. For the results in Figures 1 and 2 below, the right hand side of (30) falls in the range 1.0004 to 1.008.

3.1 Least Squares Inversion

In order to carry out least squares inversion of (28), we project the slowness perturbation $\delta s(z)$ onto the space of functions $K_n(z)$:

$$\delta s(z)\Big|_K = \sum_n A_n K_n(z). \tag{31}$$

Coefficients A_n are then determined by least squares minimization of the difference between $\delta s(z)$ and the right hand side of (31). Invoking (28), the result is

$$\mathbf{A} = \mathbf{C^{-1}}\delta\mathbf{s^g}, \tag{32}$$

where the kernel correlation matrix $\mathbf{C}$ is given by

$$C_{nm} \equiv \int K_n(z) K_m(z) dz. \tag{33}$$

The inversion is now summarized as

$$\delta s(z) \simeq \mathbf{K}(z)^T \mathbf{C^{-1}}\delta\mathbf{s^g}. \tag{34}$$

Equations (30) - (34) give the approximate inversion of group slowness data to yield the slowness perturbation in the water column, and are consistent with the range-integrated formulation of Shang[3].

4

Group Slowness Kernels for Various Environments

In Figure 1 (a) are shown the first eight eigenmodes at a frequency of 70Hz for a Munk sound speed profile with parameters $z_o = 1000m, B = 1300m$, $\epsilon = .0113$, $\eta = (z - z_o)/(B/2)$, $c_o = 1480$ m/s:

$$c(z) = c_o \left[1 + \epsilon(\eta + e^{-\eta} - 1)\right], \tag{35}$$

where z is taken to be positive downward. Figure 1 (b) gives the corresponding inversion kernels $K_n(z)$ as calculated from (29). The equivalent ray turning points, where the modal phase speed equals the local sound apeed, are marked on the eigenfunctions and on the $K_n(z)$ for comparison. The $K_n(z)$ in Figure 1 (b) have dimensions of inverse meters, with the full width of the abscissa representing 0.5m^{-1}.

The $K_n(z)$ occupy approximately the same vertical extent as the eigenfunctions $\psi_n(z)$, but oscillate roughly twice as many times. This is to be expected from the quadratic dependence of K_n upon ψ_n in (29). The negative extrema in the higher modes result from the operator inverse term in (29). Figures 1 (c,d) are the eigenmodes and $K_n(z)$ for a smoothly varying deep water sound channel typical of January near Ascension Island[15], where some HIFT data were taken. The two smooth deep water sound speed profiles of Figures 1 (a,c) result in quite similar eigenmodes and inversion kernels. For this reason we will use the Munk profile in estimating the accuracy of the perturbative approach to ocean tomography in Section 5.

In all the examples in this section, the group kernel has its first minimum (coming up from the bottom) just below the lower ray turning point for the mode under consideration (*i.e.*, just below the lowest inflection point in ψ_n), and then has a large maximum just above the first extremum in ψ_n. Strong surface interaction and double ducting to be considered below complicate the near- surface behavior of K_n.

Figures 2(a,b) illustrate a sound speed typical of the near- polar oceans with strongly surface interacting modes. The SSP is from Levitus[16] for a point near Heard Island (53S, 74E), where the ocean is 1500m deep. Below 1500m we have extended the profile by assuming a hydrostatic sound speed gradient. The modes shown are not bottom interacting, so this extension of the SSP does not affect the results. The

amplitude of K_n for this surface- limited SSP is larger than either of the two deep ocean SSP's illustrated, indicative of high dispersion.

Figures 2(c-d) show an SSP with a double duct typical of a point (44S, 41E) northwest of Crozet Island in January[17]. Modes 7 and 8 are partially trapped in the duct, and show increased group slowness sensitivity near the secondary duct.

For a smooth deep water SSP such as that of Figures 1(a,c), modal group slowness sensitivity to water column slowness is greatest near outer inflection points (corresponding to ray turning points). The highly dispersive SSP of Figures 2(a,b) shows about three times the sensitivity as the smooth deep water case. But again, maximum sensitivity occurs just inside the ray turning point locations. Double ducting (Figures 2(c,d)) complicates the relation between water column perturbations and group slowness response. There is only weak sensitivity in the upper water column for modes 2 - 6 (Figure 2(d)), but modal resonances with the secondary duct produce large responses of opposite sign for modes 7 and 8.

The results of Figures 1 and 2 support the unsurprising conclusion that group slowness perturbations are most sensitive to sound speed changes near turning points in a ray description, but with the added complication that the sign of the inversion kernel near the turning points may be positive or negative in a double ducted SSP.

The formalism provided here gives information about the projection of slowness perturbations $\delta s(z)$ on the non orthogonal oscillatory functions $K_n(z)$, whose behavior is illustrated in the right hand panels of Figures 1 and 2. For a mid latitude SSP such as that of Figure 1 (c) the response of the modal group slowness to slowness changes in the water column is weak, and peaks at upper and lower turning points. The more restricted polar SSP of Figure 2 (a) reveals increased sensitivity of the group slowness to $\delta s(z)$ due to the vertical confinement of the eigenmodes. The double ducted SSP of Figure 2 (c) shows increased sensitivity in modes which are partially trapped in the near- surface ducts. In a previous investigation [13] correlation matrices $\mathbf{C}$ for three of the above SSP's were investigated, and were found to be diagonally dominant (the Munk profile of Figure 1 (a) was not considered in that work). This reflects the general well- conditionedness of the least squares inversion technique.

As one considers higher and higher mode numbers, one finds a transition from mode trapping near the sound axis to strong surface interaction. This is illustrated for the Munk SSP in Figure 3 where the K_n for the first 60 modes are given. One sees a monotonic tendency of the group slowness kernel to become strong approaching the lower turning point, and weak near the surface. In a ray description this would correspond to a surface interacting ray spending more time near the turning point than near the surface.

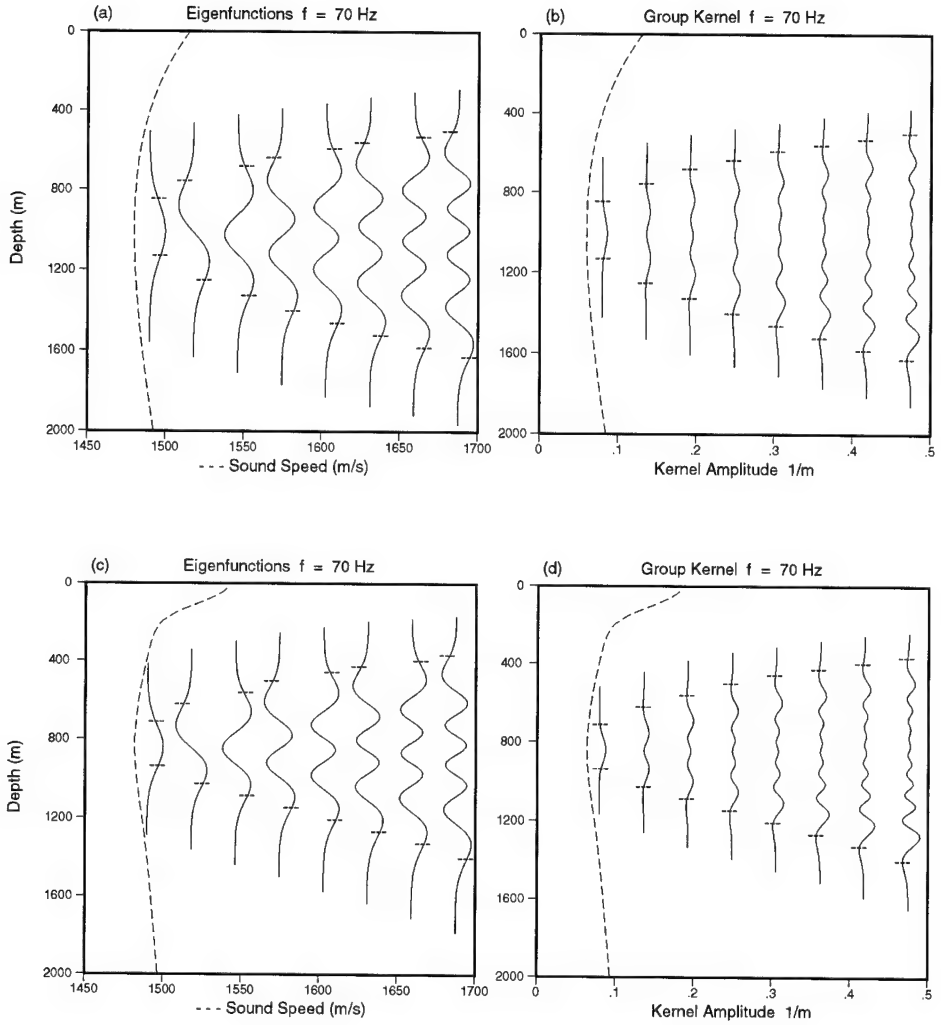

Figure 1 *(a) The first 8 eigenmodes and (b) group slowness kernels for the Munk profile of eq. (35). (c) Eigenmodes and (d) group slowness kernels for an SSP taken near Ascension Island in January. The horizontal marks on each plot give the upper and lower ray turning points. Each plot is terminated where the amplitude of the function permanently falls below .001 times its maximum amplitude.*

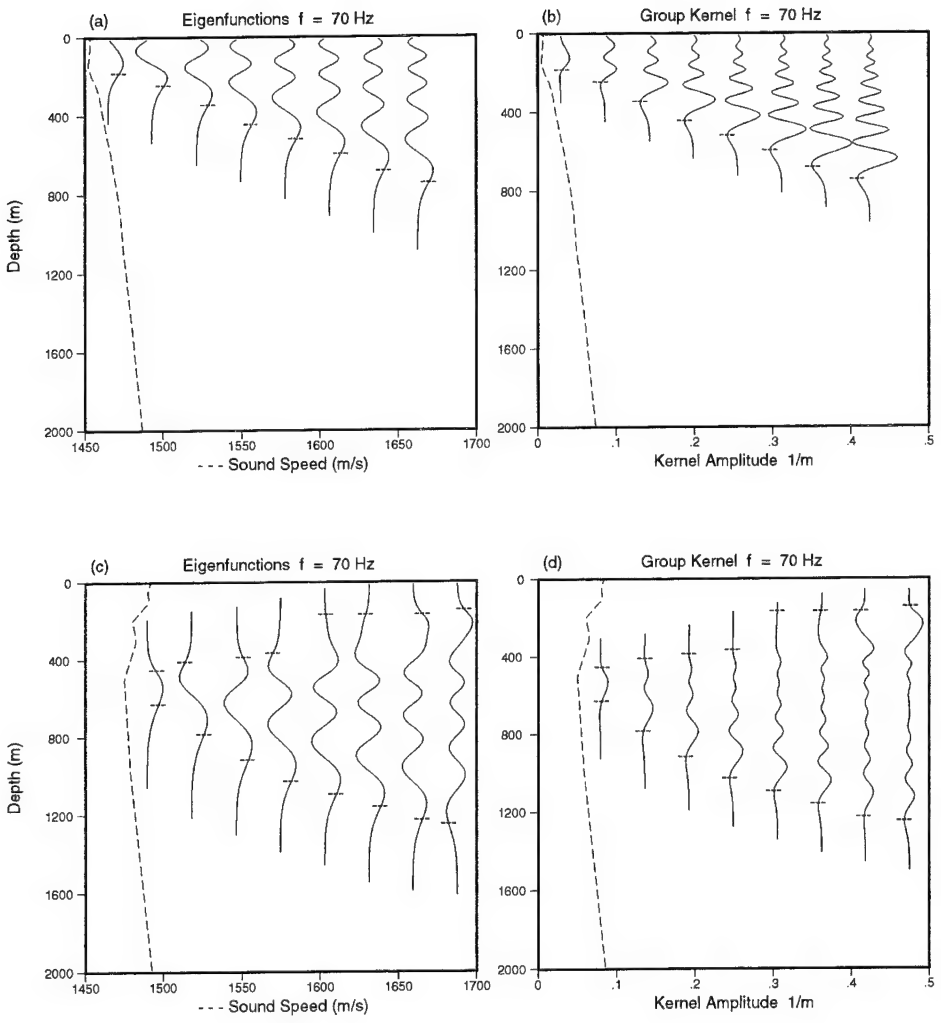

Figure 2 *(a) and (b): Results for a near - polar SSP with strong surface interaction. (c) and (d): Results for a double ducted SSP. Other details are as in Figure 1.*

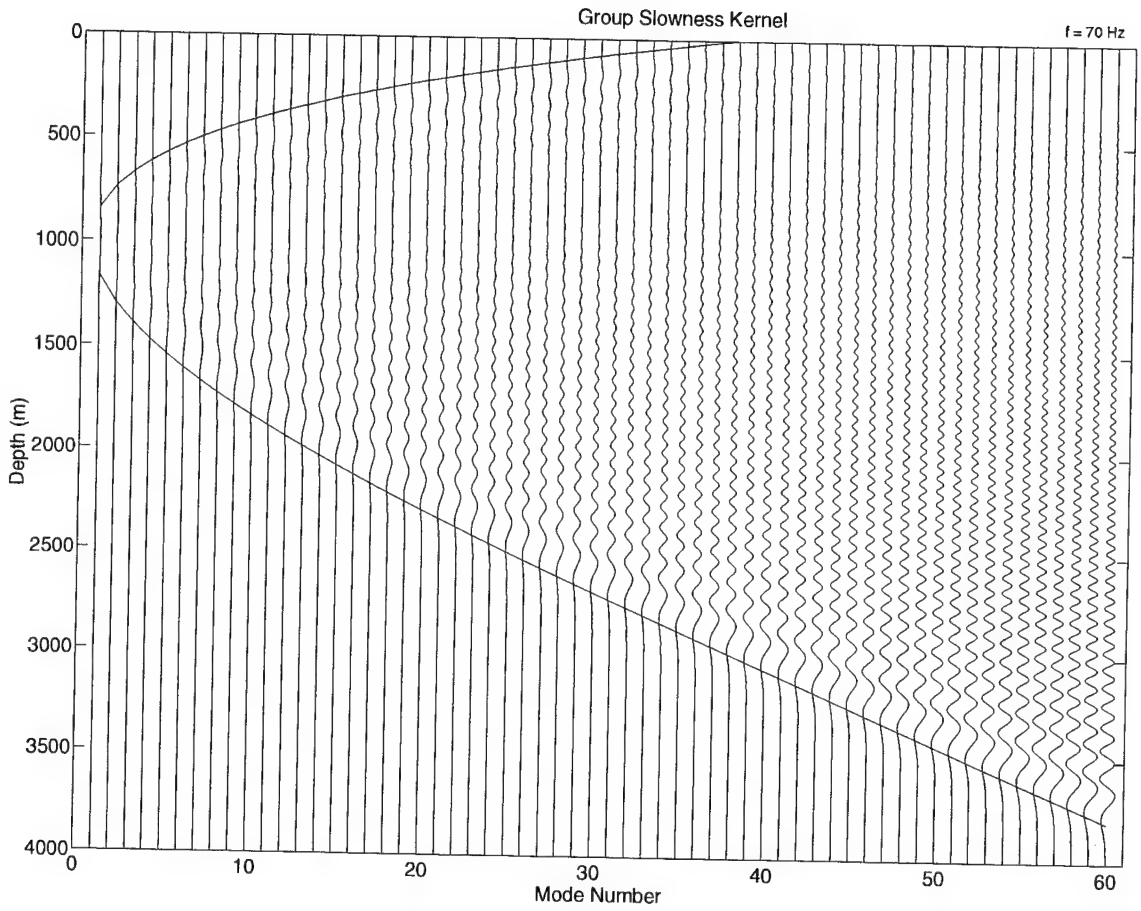

Figure 3 *Group slowness kernel K_n for the first 60 modes resulting from the Munk SSP of eq. (35). Upper and lower turning depths for each mode are indicated by curved lines.*

5

Limitations on the Linear Perturbation Method

We will now give some numerical examples in which perturbation theory results are accurate, followed by some in which the accuracy is degraded. Further studies of the parameter region in which one may use perturbation theory are underway and will be published elsewhere. The first example will compare δs_n^g as determined from (28) with that found by solving equations (1) and (14) for two different environments whose sound slowness differs by $\delta s(z)$. The eigenmodes were computed using Kraken[18]. The unperturbed case is taken to be that of the Munk SSP of eq. (35). A Hanning window was used to create the perturbation signal with a given amplitude, extent and depth location:

$$\delta s(z) = \begin{cases} \alpha \cos^2(\frac{\pi(z-z_p)}{\Delta w}) & |z - z_p| < \Delta w/2 \\ 0 & |z - z_p| > \Delta w/2 \end{cases} \tag{36}$$

Figure 4 shows δs_n^g for $\Delta w = 50m$ and amplitude $\alpha = -1 \times 10^{-6} s/m$, leading to a peak sound speed perturbation of about 2.25 m/s. The $50m$ width is smaller than most vertical correlation scales encountered in the deep ocean and is used mainly to illustrate a case of good qualitative agreement between the linear and exact methods. The linear perturbation result of Figure 4 (a) accurately method captures the high frequency structure seen in the higher modes. In fact one can match the oscillations in Figure 4 (a) to those seen in Figure 3. The smallest oscillation has a vertical wavelength of about 60 m, on par with the 50 m perturbation scale. The actual perturbation seen in Figure 4 (b) as computed from equations (1) and (14) for the two different environments is almost indistinguishable from the linear perturbation result (28).

Next we give an example in which the linearized and exact group slowness perturbations are considerably different. Figure 5 gives results for slowness perturbations in the water column as in Figure 4, but with the Hanning width increased to 200m. We show linear versus actual results δs_n^g for mode 9 in Figure 5 (a) and for mode 21 in Figure 5 (b). One sees that the linear result for these modes is off by approximately 30% to 50% with the highest errors occuring when the perturbation is near the modal turning points. The error is oscillatory with a vertical wavelength comparable to that of the group slowness kernel.

If a perturbation width of 50m gives good agreement between linear and exact results, we must ask why an increase to 200m produces such poor agreement. After

all, one could approximate the 200m width window by a linear superposition of 50m windows properly spaced. The answer is that that δs_n^g is not linear with respect to changes in the environment, so that a linear approximation must begin to fail somewhere. By enlarging the width from 50 to 200m we have perturbed more of the water column, even if the pointwise changes in the water column are of the same magnitude.

To illustrate the onset of nonlinear dependence of δs_n^g on perturbation amplitude and width, we give in Figure 6 (a) the difference between linear and actual δs_n^g for mode 9 as a function of both these parameters with the depth of the perturbation kept constant at 250m. This depth is above the upper turning point of mode 9 by approximately 250m. One sees that as the perturbation amplitude increases from zero, the error in the linear expression (28) develops a strong maximum for $\Delta w = 500$m and $\alpha = 3 \times 10^{-6}$ s/m. Then for $\Delta > 1000$m, the error is negative for both positive and negative α. A contour is drawn where the amplitude of the group slowness error is 10^{-8} s/m, corresponding to travel time accuracy of 10ms per 1000km. This level is a nominal figure for accurate ocean basin scale acoustic tomography. For mode 9 at the stated perturbation depth of 250m, the slowness perturbation amplitude needs to be smaller than approximately 10^{-6} s/m to achieve this nominal level of accuracy for the linear expression (28).

Figure 6 (b) repeats the calculation of Figure 6 (a) for mode 21. Here the error in the linear expression is always negative, and the amplitude limit for the nominal accuracy level is even more restrictive on α for perturbation widths $\Delta w < 800$m. For $\Delta w > 800$m, the nominal amplitude limit $\alpha < 10^{-6}$ s/m still applies for the linear method to give group slowness accuracy within 10^{-8} s/m. The consistent negative bias for the linear method at large vertical scale lengths Δw implies, at least for the modes under consideration, that the linear method may give biased group slowness perturbations even for a horizontally zero- mean field of water column perturbations.

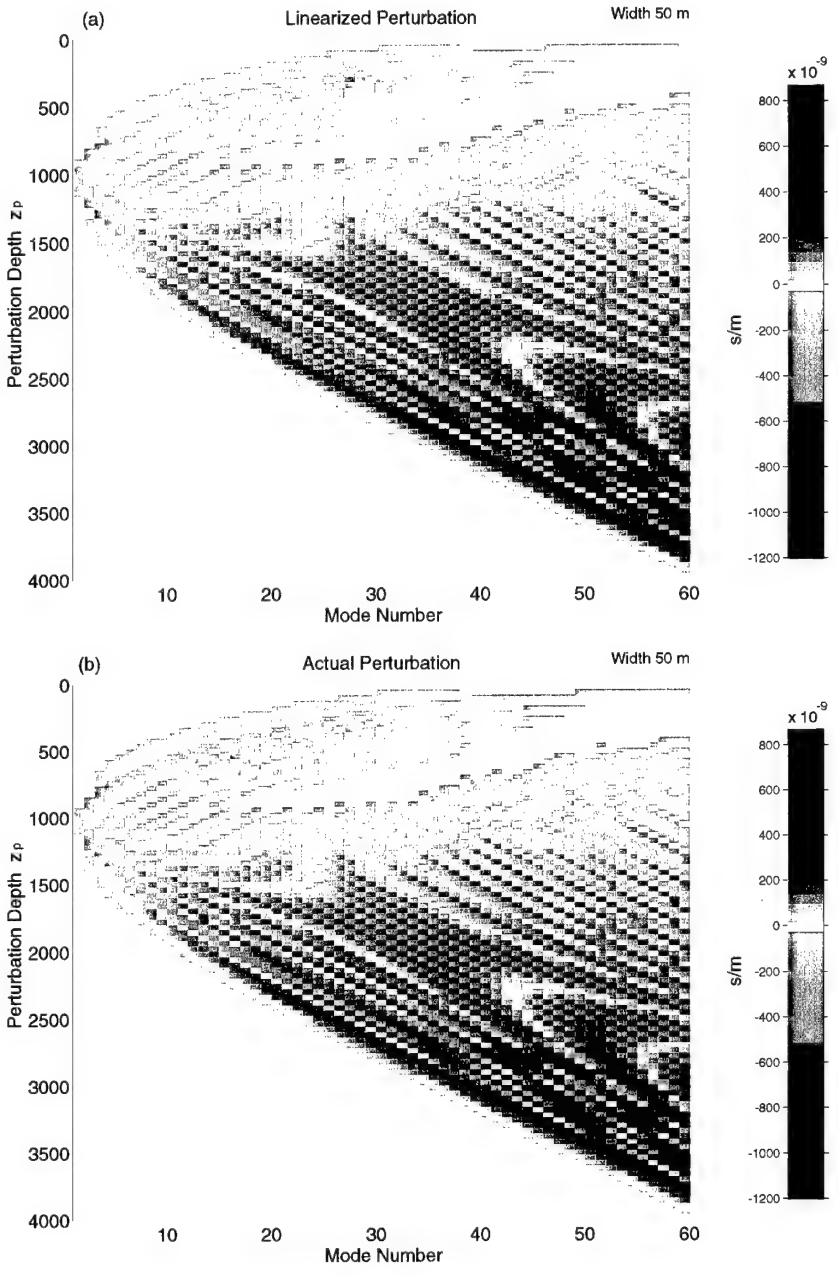

Figure 4 *(a) Linearized group slowness perturbation at 70Hz from (28) for a Hanning window perturbation (36) of the Munk SSP; (b) Actual group slowness change calculated directly from the two different SSP's.*

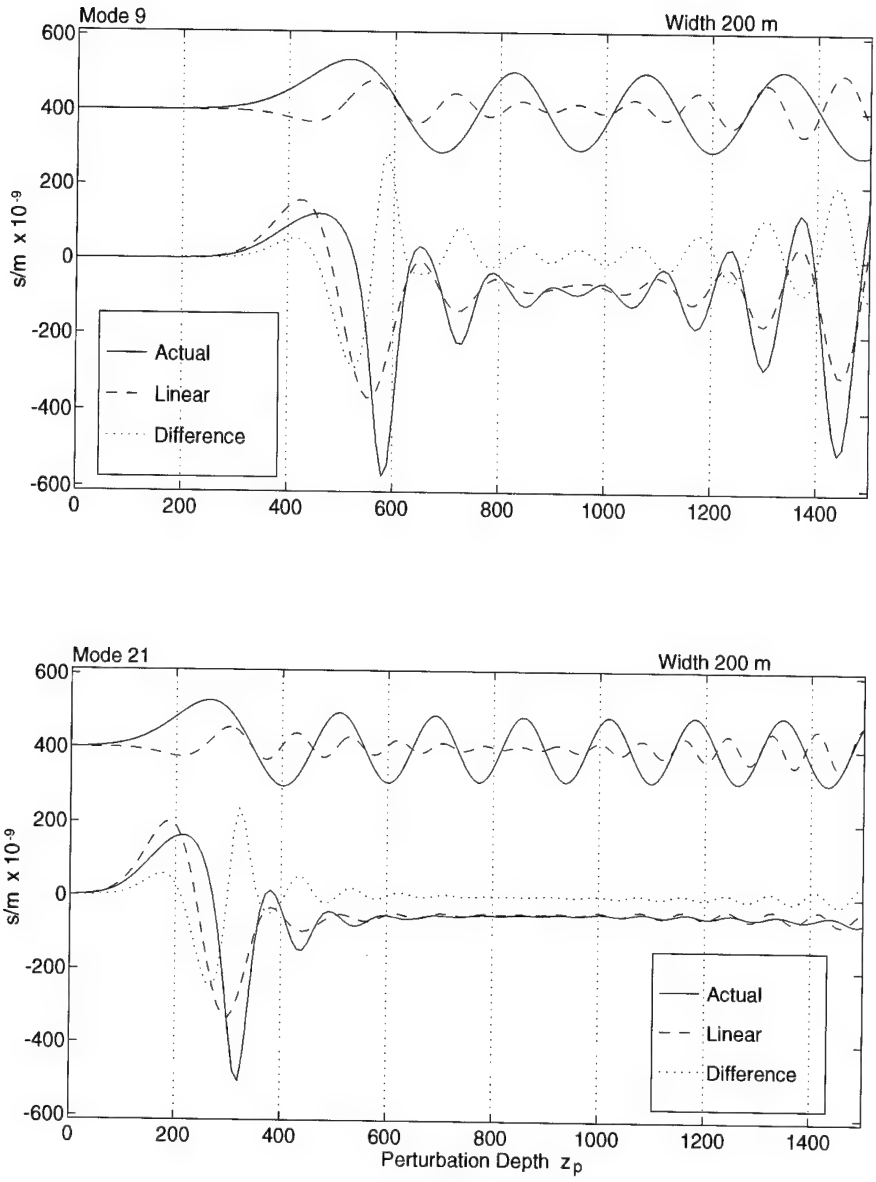

Figure 5 *Linear and actual group slowness perturbations for a 200m width Hanning perturbation pulse for modes 9 and 21 at 70Hz. The upper two curves in each plot are the unperturbed modeshape $\psi_n(z)$ (solid line) and the group slowness kernel $K_n(z)$ (dashed). Below those are three lines, giving the actual δs_n^g (solid), linearized version (dashed) and their difference (dotted).*

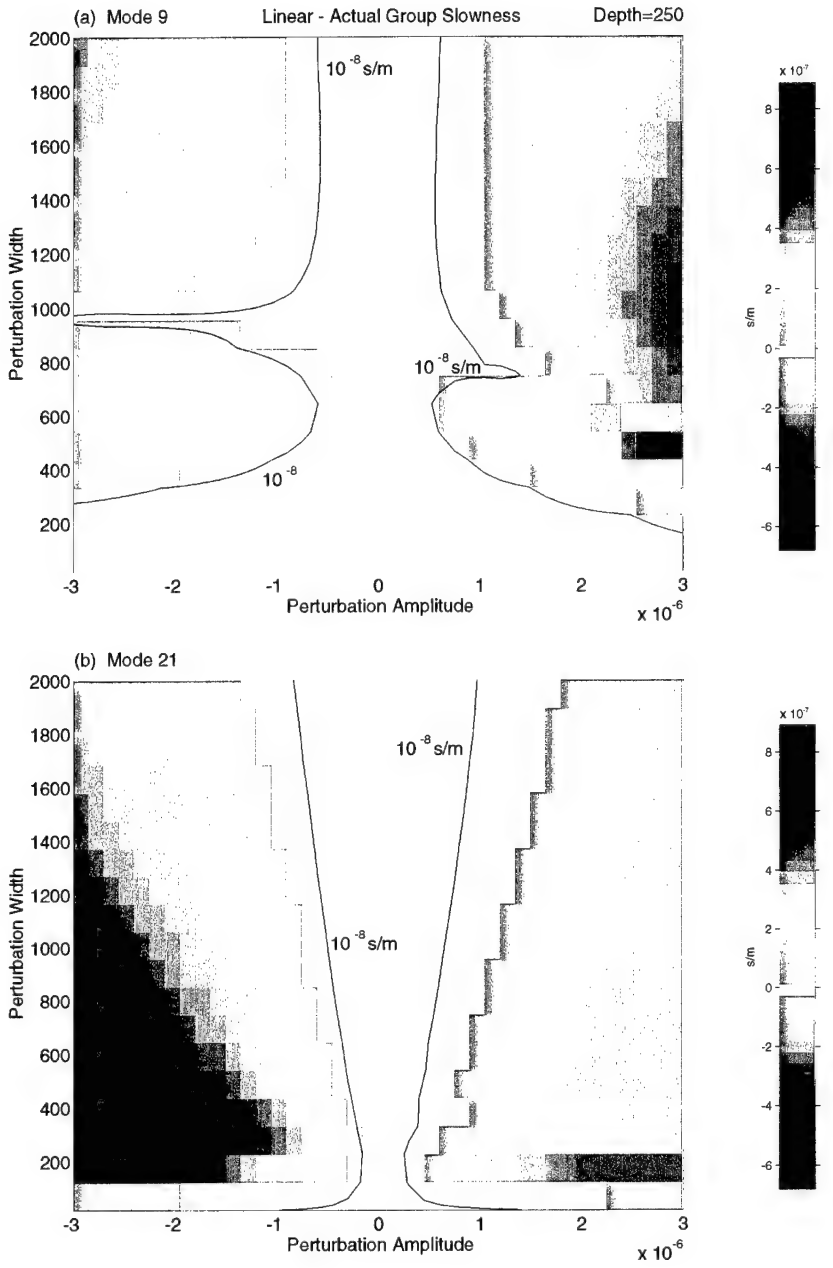

Figure 6 *Error in the linear result for group slowness perturbation at 70Hz for modes 9 (top) and 21 (bottom) as a function of perturbation width Δw and amplitude α. The perturbation to the sound slowness profile is centered at a depth of 250m. The black contour shows the region in which the error is smaller than the nominal value 10^{-8} s/m, considered acceptable for ocean basin scale tomography.*

6

Summary

We have demonstrated that the 'third term problem' stated in equation (16), which one encounters in ocean acoustic inversion, is an identity which emerges as an inherent property of Sturm - Liouville systems such as equation (1) for ocean acoustic eigenmodes. This result establishes a fundamental but not obvious role played by the eigenmode's frequency derivative in relating a water column perturbation to the eigenmode's response. We have given a method for evaluating the frequency derivative of the eigenmode which may be a useful alternative to finite differences.

When linear perturbation theory may be used, we have expressed modal group slowness changes as an integral equation (28) in $\delta s(z)$, the water column sound slowness perturbation. Equations (29) - (34) give an approximate least squares inversion for $\delta s(z)$ in terms of the modal group slowness perturbations which is consistent with that of ref[3].

The kernel of the integral equation has been given numerically in Figures 1 and 2 for four sound speed profiles: The Munk SSP, a smooth mid- latitude SSP, a mostly upward refracting high latitude SSP with strong surface interaction, and a double-ducted high latitude SSP. The first two SSP's show similar response to water column perturbations, but the last two show increased sensitivity at the lower turning point for the high latitude SSP, and in the surface ducts for the last SSP considered.

We then examined the accuracy of the linear perturbation method and found decreased accuracy at large perturbation amplitude ($|\delta s(z)| \gtrsim 10^{-6}$s/m for which $|\delta c(z)| \gtrsim 2.25$m/s) *and* at large vertical perturbation width ($\Delta w \gtrsim 50$m) for the modes considered. We also found that for large perturbation width the linear perturbation method gave biased results. It appears from other work (not presented here but under investigation for future publication) that the sign of the bias may depend on whether the water column perturbation is inside or outside the modal turning points.

References

[1] W. H. Munk and C. Wunsch, "Ocean acoustic tomography: A scheme for large-scale monitoring," *Deep Sea Res.* **26 A** 123 - 161, 1979.

[2] W. Munk, P. Worcester, and C. Wunsch, *Ocean Acoustic Tomography*, Cambridge Univ. Press, London, 1995.

[3] E. C. Shang, "Ocean acoustic tomography based on adiabatic mode theory," *J. Acoust. Soc. Am.* **85**, 1531 - 1537 (1989).

[4] A. B. Baggeroer, J. Miller, C. S. Chiu, G. Froger, P. N. Mikhalevsky, and K. von der Heydt, "Vertical array resolution of the normal modes from the Heard Island signals," *J. Acoust. Soc. Am.* **90**, 2330, (1991).

[5] W. H. Munk, "Acoustic thermometry of ocean climate," J. Acoust. Soc. Am. **100**, 2580, 1996.

[6] B. M. Howe, J. A. Mercer, R. C. Spindel, P. F. Worcester, J. A. Hildebrand, W. S. Hodgkiss, Jr., T. F. Duda, and S. M. Flattè, "SLICE89: a single slice tomography experiment," pp. 81- 86, *Ocean Variability and Propagation*, ed. J. Potter and A. Warn- Varnas, Dordrecht: Kluwer, 1991.

[7] B. E. McDonald, M. D. Collins, W. A. Kuperman, and K. D. Heaney, "Comparison of data and model predictions for Heard Island acoustic transmissions," *J. Acoust. Soc. Am.* , **96**, 2357 - 2370, 1994.

[8] K. D. Heaney, J. Colosi, and W. A. Kuperman, "Estimation of internal wave strength from mode space source localization," J. Acoust. Soc. Am. **100**, 2582, 1996.

[9] S. Rajan, J. F. Lynch, and G. V. Frisk, "Perturbative inversion methods for obtaining bottom geoacoustic parameters in shallow water," *J. Acoust. Soc. Am.* **82**, 998 - 1017, 1987.

[10] B. E. McDonald and A. B. Baggeroer, "Modal eigenfunction perturbations and group speed tomography," *J. Acoust. Soc. Am.* **94**, 1794, 1993.

[11] E. C. Shang and Y. Y. Wang, "On the calculation of modal travel time perturbation," *Sov. Phys. Acoust.* **37**, 411- 413, 1991.

[12] W. L. Rodi, P. Glover, T. M. C. Li, and S. S. Alexander, "A fast, accurate method for computing group velocity partial derivatives for Rayleigh and Love modes," *Bull. Seism. Soc. Am.*, **65**, 1105 - 1114, 1975.

[13] B. E. McDonald, "The inversion kernel in group travel time tomography," *Full Field Inversion Methods in Ocean and Seismo Acoustics*, Proc. NATO Conference, Saclant Center, La Spezia Italy, 27 June - 1 July 1994, ed. Diachok, Caiti, Gerstoft, and Schmidt, Kluwer Academic Publishers, Dordrecht, 1995.

[14] K. D. LePage, "Time series variability in fluctuating ocean waveguides," Saclantcen Report SR-319, July, 1999.

[15] Palmer. D. (1993) personal communication.

[16] Levitus, S. (1982) Climatological Atlas of the World Ocean, *NOAA prof. paper 13*, U.S. Government Printing Office, Washington DC, 173pp.

[17] Sergei Gorshov, ed. (1979) *World Ocean Atlas*, Pergamon Press.

[18] Michael B. Porter and Edward L. Reiss, "A numerical method for ocean acoustic normal modes," *J. Acoustical Soc. Am.* **76**, 244 - 252, 1984.

Document Data Sheet

Security Classification		Project No.
UNCLASSIFIED		01-A
Document Serial No.	**Date of Issue**	**Total Pages**
SR-333	August 2000	22 pp.

Author(s)

McDonald, B.E., Sperry, B., Baggeroer, A.B.

Title

Theoretical and numerical issues in travel time tomography

Abstract

Results from perturbation theory for changes in ocean acoustic modal group speeds due to small environmental changes are investigated with regard to their applicability to inversion schemes for large scale trends in the ocean's thermal structure. In regions where adiabatic mode theory is applicable, the inverse problem for each vertical eigenmode consists of an integral equation whose kernel involves the eigenfunction and its frequency derivative. We give a proof for the so called `third term problem' which requires equivalence between two dissimilar integrals relating the perturbations in the water column, the resulting perturbations in the acoustic eigenmode under consideration, and the frequency derivative of the eigenmode. We give numerical examples for the inversion kernel for four types of sound speed profiles, and then explore numerically the parameter range (amplitude and scale size) in which perturbation theory is accurate.

Keywords

perturbation theory - acoustic inversion - ocean tomography

Issuing Organization

North Atlantic Treaty Organization
SACLANT Undersea Research Centre
Viale San Bartolomeo 400, 19138 La Spezia, Italy

[From N. America: SACLANTCEN (New York) APO AE 09613]

Tel: +39 0187 527 361
Fax:+39 0187 527 700

E-mail: library@saclantc.nato.int

The SACLANT Undersea Research Centre provides the Supreme Allied Commander Atlantic (SACLANT) with scientific and technical assistance under the terms of its NATO charter, which entered into force on 1 February 1963. Without prejudice to this main task - and under the policy direction of SACLANT - the Centre also renders scientific and technical assistance to the individual NATO nations.

This document is approved for public release.
Distribution is unlimited

SACLANT Undersea Research Centre
Viale San Bartolomeo 400
19138 San Bartolomeo (SP), Italy

tel: +39 0187 527 (1) or extension
fax: +39 0187 527 700

e-mail: library@saclantc.nato.int

NORTH ATLANTIC TREATY ORGANIZATION